PHYSICAL REVIEW B **79**, 125434 (2009)

Density functional theory study of the initial oxidation of the Pt(111) surface

Jeffery M. Hawkins, Jason F. Weaver, and Aravind Asthagiri*
Department of Chemical Engineering, University of Florida, Gainesville, Florida 32611, USA
(Received 18 November 2008; revised manuscript received 6 February 2009; published 27 March 2009)

We used density functional theory calculations to examine the initial stages of oxidation of the Pt(111) surface. Consistent with prior studies, our calculations predict that oxygen atoms adsorb on fcc sites and form $p(2\times2)$ and $p(2\times1)$ structures at coverages of 0.25 and 0.50 ML, respectively. In addition to various surface configurations of oxygen on fcc sites, we examined subsurface oxygen and clustering of oxygen atoms on the surface. We find that subsurface oxygen is not the precursor to the oxidation of the Pt(111) surface. Instead, we predict a strong preference for the formation and growth of one-dimensional Pt oxide chains within the $p(2\times1)$ structure. In particular, at coverages above 0.50 ML, additional oxygen atoms prefer to aggregate between the close-packed oxygen rows formed by the $p(2\times1)$ structure and induce large buckling ($\sim$1.8 Å) and modification of the charge of the surface Pt atoms. The result is an oxide compound with threefold and fourfold Pt-O coordination that grows as a one-dimensional chain running parallel to the oxygen rows of the $p(2\times1)$ structure. Furthermore, half of the oxygen atoms in the Pt oxide chains reside near hcp sites, contrary to some reports that oxygen atoms reside only on the fcc sites on Pt(111). Our results agree well with a recent scanning tunneling microscopy study and suggest a precursor mechanism to the oxidation of metal surfaces involving Pt oxide chain formation and growth on terraces at moderate oxygen coverages. Our results should have important implications to current models of NO and CO oxidation on Pt(111) and potentially on studies of the initial oxidation of other transition-metal and bimetallic surfaces.

DOI: 10.1103/PhysRevB.79.125434 PACS number(s): 73.22.−f, 81.65.Mq

I. INTRODUCTION

Understanding the oxidation behavior of platinum and other late transition metals (TMs) is important since these metals are used in several industrially important oxygen-rich catalytic processes, such as the selective oxidation of organic compounds, oxidation of NO to NO_2, and combustion exhaust remediation. An atomic-level understanding of the changes to the TM surface under oxygen-rich conditions would be useful in interpreting and optimizing catalyst behavior under reaction conditions. Fundamental surface science studies in ultrahigh vacuum (UHV) of the oxidation of Pt surfaces are complicated by the low sticking coefficient of O_2, which results in the so-called pressure gap.[1] Using molecular oxygen, surface oxygen coverages are restricted to 0.25 ML (monolayers), which is an insufficient coverage to probe the transition from a surface chemisorbed oxygen phase to the formation of surface oxide(s). The coverage limit can be circumvented by the use of more aggressive oxidants, such as NO_2,[2] ozone,[3] atomic oxygen,[4–6] or high-pressure cells.[7] Scanning tunneling microscopy (STM) has had a particularly significant impact on our understanding of oxide phases on several TM surfaces. Recently, combined STM and density functional theory (DFT) studies have resolved two-dimensional (2D) oxide phases on Rh(111) (Refs. 8 and 9) and Pd(111).[10,11]

Several groups have probed oxygen on the Pt(111) surface in UHV with temperature programmed desorption (TPD), x-ray photoelectron spectroscopy (XPS), and low-energy electron diffraction (LEED),[2,5,6] as well as by using a combination of DFT (Refs. 12–15) and cluster expansion based Monte Carlo (MC).[16,17] At coverages below 0.25 ML, the O atoms adsorb on fcc hollow sites and form a $p(2\times2)$ surface structure. This structure maintains maximum distance between the O atoms at 0.25 ML coverage and minimizes the O-O repulsion. DFT calculations have shown that the O binding energy declines with increasing O surface coverage.[12–15] Subsequent increases in the surface coverage above 0.25 ML show the development of a series of different O phases as indicated by differences in the O_2 TPD spectra.[2,5,6] TPD data show three unique states, labeled β_1, β_2, and β_3, which appear as the surface coverage is increased from 0 to 0.75 ML. The aforementioned $p(2\times2)$ structure (β_3) appears first, and the peak associated with this state shifts downward in temperature as the coverage is increased from 0 to 0.25 ML, indicative of the O-O repulsion. As the coverage is increased beyond 0.25 ML, a second peak (β_2) starts to form as a shoulder to the β_3 peak and grows in intensity from 0.25 to 0.5 ML. At the same stage the β_2 peak starts to appear, the LEED pattern associated with the $p(2\times2)$ starts to fade and disappears rapidly above 0.5 ML. Unfortunately, a clear structure cannot be resolved based on the LEED for the β_2 phase, but researchers have postulated two possible structures.[2,5,18] In the first possible structure, the O atoms continue to occupy fcc sites and arrange into a $p(2\times1)$ structure. The (2×2) LEED pattern can match this structure if three rotationally degenerate $p(2\times1)$ domains co-exist.[2,5] In the alternative structure, additional O atoms adsorbed on the $p(2\times2)$ structure bind on hcp hollow sites, producing a honeycomb structure. TPD spectra obtained using a mixture of ^{18}O and ^{16}O atoms provide evidence that oxygen atoms adsorb on different sites above 0.25 ML.[18] This result suggests that the honeycomb structure is associated with the β_2 state. DFT calculations by several groups contradict this conclusion and predict that the $p(2\times1)$ structure is favored over occupation of the hcp site by 0.5 eV.[12–15] A recent STM study has resolved this controversy,[19] revealing $p(2\times1)$ domains of oxygen atoms below 0.5 ML. We

will return to the results from that work later in Sec. III since it plays an important role in our approach to examining O surface structures in this paper. Further increases in the surface coverage from 0.5 to 0.75 ML introduce yet another desorption peak (β_1), which appears at a lower temperature than the other two peaks. The atomic-level structure of the β_1 state was unknown until the recent STM work by Devarajan *et al.*[19]

Several DFT studies have attempted to resolve the behavior of O beyond 0.25 ML and provide the missing structural information about higher coverage oxygen phases on Pt(111). The approach has been to generate all possible structures of oxygen on the Pt(111) surface and evaluate the energetics (or thermodynamics) of the various structures. To make these studies practical, restrictions must be made on the possible structures for the oxygen adlayer. The primary assumptions have been to restrict the structures to chemisorbed O on the surface, and in some studies, to restrict the O binding sites to the fcc hollow. As noted above, DFT calculations indicate that the hcp hollow is not favored over the fcc hollow at 0.5 ML, and test calculations at higher coverages seem to support this assumption.[13,16,17] While the majority of the DFT studies of O/Pt(111) focus on surface oxygen, Légaré[12] examined structures with a mixture of surface and subsurface oxygen. Todorova and co-workers[20] demonstrated using DFT that subsurface oxygen becomes favorable on Pd(111) at a coverage between 0.5 and 0.75 ML. Légaré predicts that subsurface oxygen becomes favored on Pt(111) at a coverage between 0.5 and 0.75 ML.[12] As we will discuss in Sec. III, we have performed similar calculations in this study that contradict the result of Légaré. A recent DFT study compared chemisorbed O structures to a 2D α-$PtO_2(0001)$ oxide film rotated 30° on Pt(111) and found the oxide film to be more stable at temperatures below around 800 K.[21,22] An *ab initio* thermodynamics study of the surface energy of the α-$PtO_2(0001)$ oxide and various surface O coverages on Pt(111) also shows that the α-$PtO_2(0001)$ oxide surface is more stable than fcc surface O coverages at oxygen chemical potentials close to the transition between $p(2\times2)$ and $p(2\times1)$ O surface configurations on Pt(111).[13] The finding that a 2D oxide is favored over chemisorbed O suggests a transition from surface O to an oxide phase, but the details of the transition coverage and the structures that form in the intermediate stages have not yet been explored computationally.

In this study, we perform DFT calculations to probe the energetics of various oxygen structures on Pt(111), and guided by recent STM results, we have discovered structures that are substantially preferred to the structures that have been reported to date. Furthermore, we have probed the kinetics for O atoms to diffuse into the subsurface. We show that the initiation of oxide growth on the Pt(111) surface does not proceed by subsurface diffusion, but instead an unexpected clustering of the O atoms occurs beyond 0.5 ML with pronounced surface buckling that results in Pt oxide chain structures on Pt(111). Our results shed light on the transition from a chemisorbed surface oxygen phase to 2D oxide structures on Pt(111), as they reveal that the formation of low-dimensional oxide structures is favored over the development of high-density chemisorbed layers or the occupation of subsurface sites.

II. CALCULATION DETAILS

All of the DFT calculations in this paper are performed using the Vienna *ab initio* simulation package (VASP).[23–26] We use the projector augmented wave (PAW) pseudopotentials[27,28] provided in the VASP database. Calculations have been done using the generalized gradient approximation Perdew-Burke-Ernzerhof (GGA-PBE) exchange-correlation functional.[29] We have also tested select calculations using the PW91 functional and find the adsorption energy is about 0.1 eV/O atom higher than the PBE values. Nevertheless, the differences between adsorption energy of configurations at the same coverage are sufficiently small that the choice of functional does not affect the results reported in this paper. In particular, the oxygen phases that we identify and discuss in Sec. III B remain the most stable phases independent of the choice of GGA functional. A plane-wave expansion with a cutoff of 400 eV is used, and the total-energy calculations are done using a block Davidson iteration method for electronic relaxations, accelerated using Methfessel-Paxton Fermi-level smearing with a Gaussian width of 0.2 eV.[30] The positions of the atoms are relaxed using a limited memory Broyden-Fletcher-Goldfarb-Shanno (LBFGS) optimization method[31] until the forces on all unconstrained atoms are less than 0.03 eV/Å. All calculations are done using a five-layer slab with a 2×2 (4×4) surface unit cell, which allows us to study O coverages in increments of 0.25 (0.0625) ML. The adsorbed O atoms and the top three Pt layers are permitted to fully relax while the lower two Pt layers are held fixed. A vacuum region of about 13 Å ensures that the slab does not interact with its periodic image in the surface-normal direction. We use a $4\times4\times1$ and $2\times2\times1$ Monkhorst-Pack mesh[32] for the 2×2 and 4×4 surface unit cells, respectively. We have confirmed that higher-energy cutoffs and finer **k**-point meshes have a negligible effect (<0.01 eV) on the binding energies reported. For example, using a $4\times4\times1$ **k**-point mesh for the 4×4 surface unit cell alters the difference in binding (total) energies of the all-fcc and oxide chain configurations at 0.75 ML [shown in Figs. 10(b) and 10(a), respectively] by 8×10^{-4} eV/O atom (0.01 eV). The lattice parameter for Pt is found to be 3.977 Å using DFT versus an experimental value of 3.92 Å.[33] All calculations reported are performed while fixing the in-plane lattice parameter to 3.977 Å. Minimum energy pathways (MEP) and barriers for chemisorbed O atoms to diffuse into the subsurface are calculated using the climbing nudged elastic band (NEB) method.[34–36]

III. RESULTS AND DISCUSSION

A. O/2×2-Pt(111)

We initially examined the energetics of O atoms in various configurations occupying surface and subsurface sites (illustrated in Fig. 1) on the 2×2 surface unit cell of Pt(111) from 0.25 to 1 ML. We discuss the stability of the various oxygen configurations in terms of the binding energy per O atom (E_b), which is given by

$$E_b = [E_{\mathrm{Pt,bare}} + n \cdot E_{\mathrm{O}_2}/2 - E_{\mathrm{O/Pt}}]/n, \quad (1)$$

where the bare Pt(111) slab and an isolated triplet O_2 molecule are used as reference states, and n indicates the number

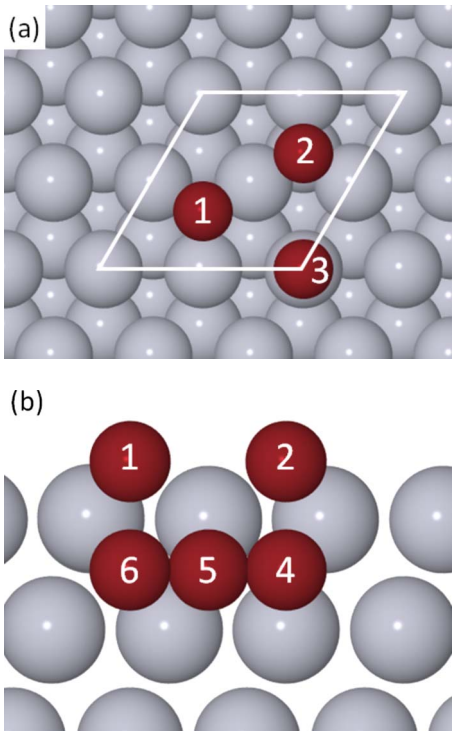

FIG. 1. (Color online) Illustration of the (a) surface and (b) subsurface adsorption sites on Pt(111), where 1=fcc, 2=hcp, 3=atop, 4=tetra-I, 5=tetra-II, and 6=octa. The 2×2 surface unit cell is shown in (a).

of O atoms adsorbed on the Pt(111) surface. By our definition of E_b, a larger positive value indicates a more stable adsorption site. We do not examine the surface free energy as a function of oxygen chemical potential (i.e., the thermodynamics) for this system because our interest is in identifying the most stable oxygen structure as a function of surface O coverage. The differences in vibrational and configurational entropy contributions between various O configurations at the same O coverage are not expected to be large enough to change the conclusions that are drawn in this paper.[12–15] The three possible surface adsorption sites are the two threefold hollow sites, the fcc (hcp) site, located above a Pt atom in the third (second) layer, and an atop site located directly above a Pt atom in the first layer. We only consider the three high-symmetry interstitial sites located between the first and second Pt layers for the subsurface incorporation of O atoms. There are two fourfold-coordinated tetrahedral sites (tetra-I and tetra-II) and one sixfold-coordinated octahedral (octa) site [see Fig. 1(b)]. The tetra-I site is located below the hcp surface site, tetra-II is below a first-layer Pt atom, and octa is below the fcc surface site.

The existence of several surface and subsurface sites leads to a multitude of possible configurations. To limit the total number of configurations, we make several restrictions, some of which are revisited when we examine O on a 4×4-Pt(111) system discussed in Sec. III B. The configurations can be split into two general types: surface and subsurface. In the surface configurations, all of the O atoms reside on the surface. At each coverage, we have examined surface configurations where all O atoms reside in the fcc, hcp, and atop sites, respectively, and mixed configurations consisting of $(n-1)$ O atoms on the fcc and one O atom on the hcp or atop sites. For the subsurface configurations, $(n-1)$ O atoms are on the surface fcc sites, and one O atom is placed in one of the three possible subsurface sites. Even with these restrictions, there are several possible configurations that need to be explored at each coverage. We note that our approach is very similar to the recent study of subsurface O on Pd(111).[20] Légaré performed a similar study of O/Pt(111) (Ref. 12) but did not examine as many surface/subsurface configurations as we report in this paper. Table I reports the binding energy for the most important configurations we have examined on the 2×2-Pt(111) surface. Configurations such as those with O atoms all on the hcp or atop sites are considerably less stable and are not reported in Table I. The top views of the favored surface configurations at each coverage are shown in Fig. 2. Figure 2(b) shows the $p(2\times1)$ surface configuration which was recently observed in STM experiments of oxygen on Pt(111).[19] There is a modest Pt buckling due to the presence of the surface O which peaks at 0.5 ML coverage before declining to zero at 1 ML. Our results for the O surface configurations match previous DFT results.[12,13,37,38] Specifically, the favored O surface configuration corresponds to O atoms residing in the fcc sites at all surface O coverages as shown in Fig. 2. Configurations generated by placing one of the O atoms in the hcp site (referred to as $(n-1)$ fcc +1 hcp in Table I) are found to have smaller binding energies. This difference in energy of pure fcc and configurations with fcc and 1 hcp decreases with increasing coverage, but even at 1 ML, the all-fcc configuration is favored by 0.04 eV/O atom. From these results, several studies in the past have concluded that the only relevant surface site is the fcc hollow. With this restriction and neglecting subsurface O atoms, the most stable O configurations can be identified,[13] and it has been reported that O atoms reside in the fcc at maximum separation to reduce the O-O repulsion.

TABLE I. Binding energies of subsurface O and surface O configurations on 2×2-Pt(111). (a),(b)=tetra-I,-II site.

Sites	Θ_{total} (ML)			
on-/ sub-surface	0.25	0.50	0.75	1.00
(n)fcc/-	1.21	0.90	0.52	0.15
$(n-1)$fcc+1 hcp/-	0.78	0.60	0.34	0.11
$(n-1)$fcc/tetra-I	−0.77	0.47	0.21(a) 0.48(b)	0.24
$(n-1)$fcc/tetra-II	−1.74	−0.25	0.26(a) −0.01(b)	0.13
$(n-1)$fcc/octa	−1.61	−0.45	0.09[a]	−0.17

[a]fcc/octa moves to hcp/octa

With the incorporation of subsurface O atoms, we can expect to have a transition from the preference of surface configurations at lower O coverages to the subsurface at sufficiently high coverage. The subsurface will become favored when the surface O-O repulsions become too large and the cost of the strain associated with subsurface O is sufficiently balanced by the screening of the O-O interactions. Table I

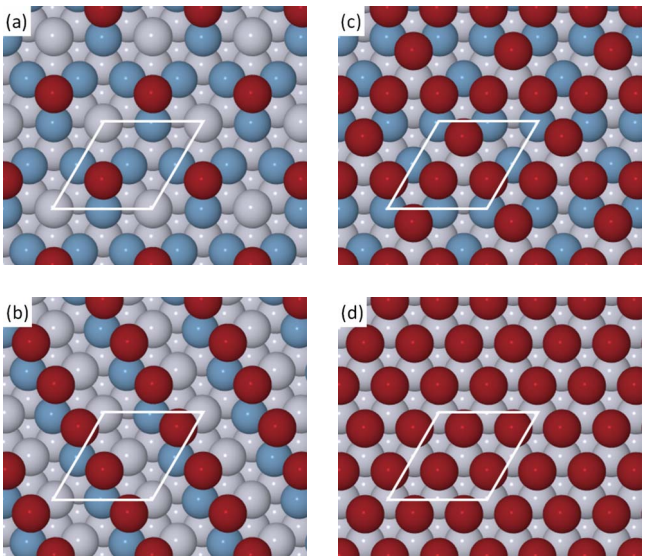

FIG. 2. (Color online) Top views of the most stable O surface-atom configuration at (a) 0.25 ML, (b) 0.50 ML, (c) 0.75 ML, and (d) 1 ML found on the 2×2 surface unit cell. The O atoms are represented by red, and the gray and blue represent the down and up buckled Pt atoms, respectively. The O atom pulls up the nearest Pt atoms, and the Pt buckling is 0.13, 0.19, and 0.04 Å for 0.25, 0.50, and 0.75 ML O coverage.

reports the values for the most stable subsurface configurations we have identified, and two general features can be observed. First, for all subsurface configurations, the tetra-I subsurface site is the most favored. Figure 3 shows the favored subsurface configurations at each coverage from 0.50 to 1 ML. As expected, there is much more significant surface Pt buckling with the presence of subsurface O atoms. The surface O atoms are screened from the subsurface O atoms by the Pt atoms, which reduces the O-O repulsion. The second observation is that the crossover between surface and subsurface configurations occurs at some coverage above 0.75 ML, as illustrated by Fig. 4, which plots the most favored surface and subsurface configurations as a function of ML of oxygen atoms. At low coverages (0.25 ML), the difference between surface and subsurface is quite large, and in fact, the subsurface O configurations are not stable. As the coverage is increased, the difference between surface and subsurface starts to drop, and by 0.75 ML coverage, the difference in binding energy is 0.04 eV/O atom. At 1 ML, the subsurface is favored by 0.09 eV/O atom, but for both the surface and subsurface, the binding energy decreases from the 0.75 ML value. We note that Légaré predicts the transition from surface to subsurface on Pt(111) to occur beyond 0.5 ML. We have examined Légaré's reported subsurface structure at 0.75 ML, which is also a tetra-I subsurface configuration, and find differences in the buckling between the two structures. We have used Légaré's structure as input, but relaxation reproduces our most favored arrangement and energy. The differences in the parameters of the DFT calculations are insufficient to cause this discrepancy, so the reasons for the structural differences are unclear. We note that the difference in binding energy between the surface and subsurface configurations at 0.25 and 0.5 ML are in relatively good

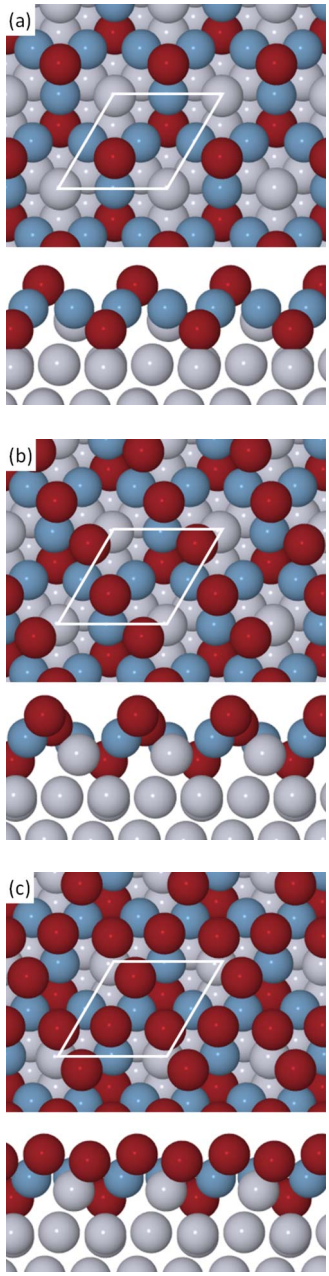

FIG. 3. (Color online) Top and side views of the most stable O subsurface atom configuration at (a) 0.50 ML, (b) 0.75 ML, and (c) 1 ML found on the 2×2 surface unit cell. The O atoms are represented by red, and the gray and blue represent the down and up buckled Pt atoms, respectively. The surface (subsurface) O atom pulls (pushes) up the nearest Pt atoms, and the Pt buckling is 0.62, 0.84, and 0.69 Å for 0.50, 0.75, and 1 ML O coverage.

agreement with the values reported in Légaré's study.

We conclude the discussion of our results on the 2×2-Pt(111) system by reporting the MEP and energy barriers to an O atom diffusing from the surface to the subsurface. The barriers and paths for subsurface O at 0.25 and 0.5 ML coverage are shown in Fig. 5. The O atom hops from the fcc to the hcp site and then diffuses into the subsurface tetra-I site. The barrier is quite large for this process at 2.23 (3.19) eV at 0.25 (0.50) ML coverage. Our value at 0.25 ML

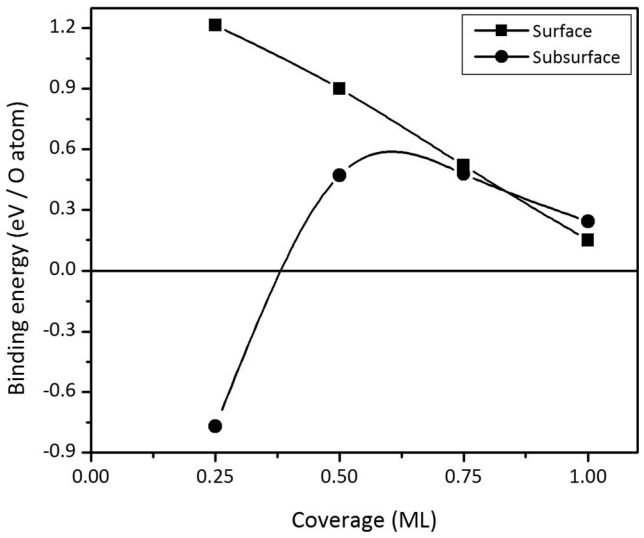

FIG. 4. Binding energy as a function of O coverage on 2×2-Pt(111) for the most stable surface (■) and subsurface (●) configurations.

agrees with a recent calculation by Gu and Balbuena.[37] We attempted to determine the barriers at 0.75 and 1 ML, but the NEB calculations failed to converge. This failure to converge is due to the very unfavorable transition state structures at these coverages. Using a 2×2-Pt(111) system causes considerable interactions between the diffusing O atom and its periodic image. A truer measure of the energy barriers for subsurface O can be obtained using larger unit cells. We revisit the barriers to subsurface O in Sec. III B when we examine O on a 4×4-Pt(111) surface unit cell.

B. O/4×4-Pt(111)

To examine more complex configurations, we turn to a 4×4-Pt(111) surface unit cell. With a 4×4 surface cell, we

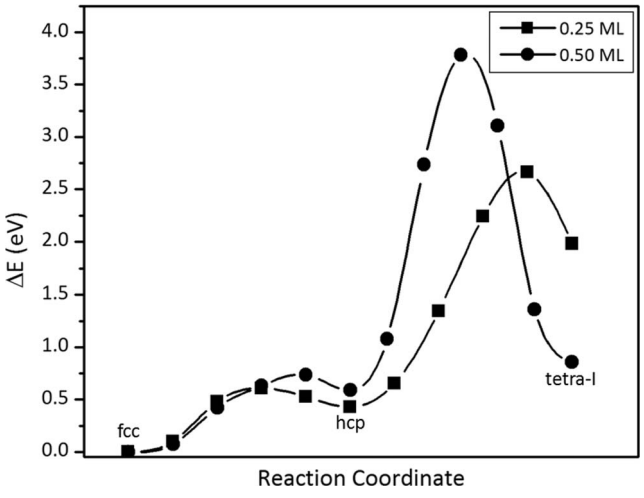

FIG. 5. The MEP for an O atom diffusing from surface fcc to subsurface tetra-I site at 0.25 ML (■) and 0.50 ML (●). The barrier for the fcc to hcp hop at 0.25 (0.50) ML is 0.61 (0.74) eV, and the barrier for diffusion from the hcp surface site to the tetra-I subsurface site at 0.25 (0.50) ML is 2.23 (3.19) eV.

can probe increments in coverage of 0.0625 ML. Furthermore, configurations where the O atoms cluster can be more readily explored in the larger system. The need to explore other configurations is motivated by recent STM images of oxygen on Pt(111) from 0.25 to 0.75 ML. In contradiction with our conclusions from Sec. III A and other DFT studies,[12,13,37] Devarajan *et al.*[19] observed O atom clustering and chain formation with pronounced surface buckling at total coverages as low as 0.4 ML. As the coverage is increased past 0.5 ML, Y-shaped structures consisting of oxide chains appear within the $p(2\times1)$ domains. The STM results reveal that the true minimum-energy configurations have not yet been identified by DFT. Rather than attempting every possible combination on the 4×4-Pt(111), we use a different approach based on the viewpoint of adding O atoms to a configuration that is in agreement with experimental results, namely, the $p(2\times1)$ configuration at 0.5 ML. The STM results clearly show that the $p(2\times1)$ structure is the dominant phase at total coverages near 0.5 ML and that the chain structures nucleate within the $p(2\times1)$ domains. We have confirmed that the energies of the configurations reported in Sec. III A for the 2×2-Pt(111) system can be reproduced exactly on the 4×4-Pt(111) system.

The first set of configurations that we explored is at 0.5625 ML coverage. At this coverage, one O atom was added to the $p(2\times1)$ structure and placed on the fcc, hcp, and atop sites, as well as the three subsurface sites. The favored surface and subsurface configurations at 0.5625 ML are shown in Fig. 6 with the added O atom clearly marked. For the subsurface configuration, the preferred site is still the tetra-I. The surface configuration is favored by 0.07 eV/O atom over the subsurface, but more interestingly, the O atom resides near an hcp site instead of an fcc site in the favored surface configuration. The additional surface O atom near the hcp site is favored over the fcc site by 0.04 eV/O atom. As seen in the favored surface configuration [Fig. 6(a)], adding an oxygen atom between the $p(2\times1)$ oxygen rows produces two Pt atoms that are threefold coordinated with oxygen atoms, two of which originate from a close-packed row of the $p(2\times1)$ structure. Interestingly, these threefold coordinated Pt atoms undergo tremendous upward buckling (1.44 Å), in good agreement with recent STM images that indicate a buckling of 1.7 Å.[19] The side view in Fig. 6(a) shows clearly that the buckled Pt atoms can serve to screen the O-O interactions on the surface. As elaborated below, the surface structure that results from adding an oxygen atom to the $p(2\times1)$ structure represents the initial building block of an oxide chain compound that preferentially develops above oxygen coverages of 0.50 ML.

Our identification of an oxide chain compound can explain prior experimental TPD results, which suggest that oxygen atoms begin to bind at sites other than the fcc hollow after saturation of the $p(2\times2)$ structure.[18] Recall from the introduction that Jerdev *et al.* suggested the presence of O atoms in hcp sites above 0.25 ML based on TPD spectra obtained after sequentially adsorbing ^{18}O and ^{16}O atoms on Pt(111). However, instead of a honeycomb structure as the source of the hcp binding sites for oxygen atoms,[18] the STM

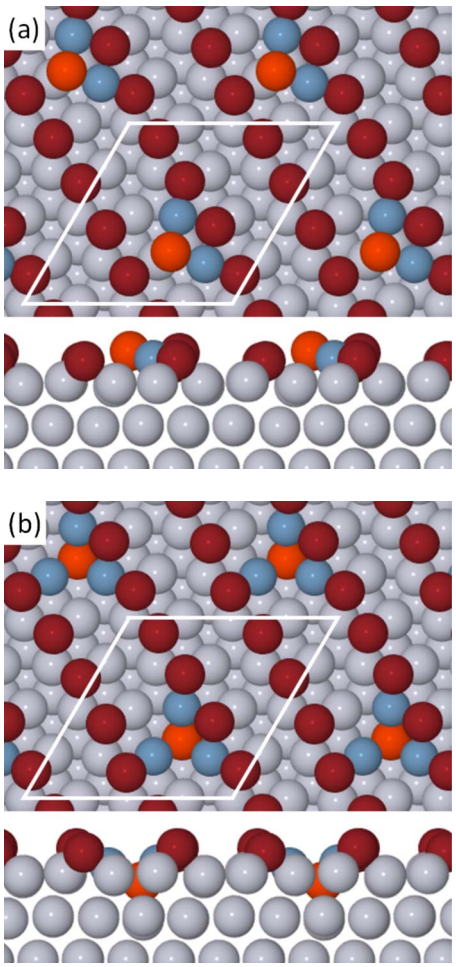

FIG. 6. (Color online) Top and side views of the most stable O (a) surface and (b) subsurface atom configuration at 0.5625 ML found on the 4×4 surface unit cell. The $p(2\times1)$ O atoms are represented by red while the additional O atom is orange. The gray and blue represent the down and up buckled Pt atoms, respectively. The additional O atom on the surface (subsurface) pulls (pushes) up the nearest Pt atoms, and the Pt buckling is 1.44 (0.75) Å.

and our DFT results suggest that the different adsorption site is associated with the nucleation of O atoms at high local coverages within the $p(2\times1)$ structure. Oxygen atoms can begin to adsorb on local domains of $p(2\times1)$ slightly above 0.25 ML, but STM results suggest that such adsorption becomes more prevalent around 0.4 ML where large domains of $p(2\times1)$ coexist with remaining domains of the $p(2\times2)$ structure.[19]

We briefly return to the MEP for subsurface oxygen that are calculated on the 4×4-Pt(111) surface cell. Figure 7 shows the barriers and MEP for subsurface oxygen at 0.25, 0.50, and 0.5625 ML. With a 4×4-Pt(111) cell at a coverage of 0.25 ML, we can examine the more realistic scenario of subsurface coverages of 0.0625 ML instead of 0.25 ML on the 2×2-Pt(111). The binding energy of such a low concentration of subsurface oxygen at total coverages of 0.25 and 0.5 ML are far more stable than the values reported for the 2×2-Pt(111) system (see Fig. 12 discussed below). As on the 2×2-Pt(111) system, the oxygen atom hops from fcc to hcp to subsurface tetra-I at coverages of 0.25 and 0.50 ML,

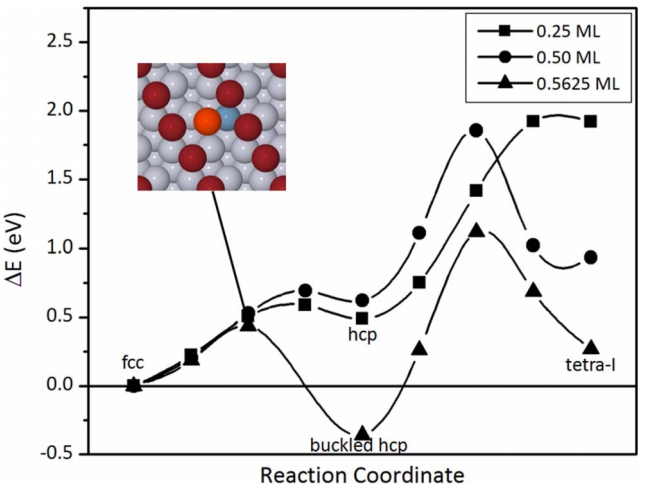

FIG. 7. (Color online) The MEP for an O atom diffusing from surface fcc to subsurface tetra-I site at 0.25 ML (■), 0.50 ML (●), and 0.5625 ML (▲) on the 4×4 surface unit cell. The barrier for the fcc to hcp hop at 0.25 (0.50) ML is 0.59 (0.69) eV, which is comparable to that on the 2×2 surface unit cell. The barrier for diffusion from the hcp surface site to the tetra-I subsurface site at 0.25 (0.50) ML is 1.43 (1.23) eV, which is notably lower than on the 2×2 surface unit cell. At 0.5625 ML, the barrier for the fcc to buckled hcp hop is 0.44 eV, and the barrier from buckled hcp to tetra-I is 1.48 eV. The transition state between fcc and buckled hcp is shown in the inset.

but the barriers are much lower on the 4×4 surface cell. The barrier from hcp to subsurface drops from 2.23 (3.19) to 1.43 (1.23) eV for 0.25 (0.50) ML when we use the larger surface cell. While we would expect that the 4×4 is sufficiently large to give the true barrier for one oxygen atom to diffuse into the subsurface at these coverages, explicitly testing this prediction through larger surface cells is beyond the scope of this paper. At 0.5625 ML, the barrier for the additional oxygen atom located between $p(2\times1)$ oxygen rows to move from the fcc to hcp site, which results in the buckled O structure shown in Fig. 6(a), is 0.44 eV. The barrier to subsurface oxygen at 0.5625 ML is 1.48 eV, which is close to the value at 0.5 ML. Given that the barriers for diffusion of oxygen into the subsurface are relatively large, these results suggest that a negligible amount of oxygen atoms will occupy subsurface sites on Pt(111) up to 0.5625 ML, and as we show below, the same holds true for higher coverages up to 1 ML.

We have also examined the favored surface and subsurface configurations at coverages from 0.5 to 0.75 ML on the 4×4-Pt(111) surface using a similar procedure as that outlined for 0.5625 ML. Our calculations reveal a strong preference for oxygen atoms to aggregate and grow a one-dimensional (1D) Pt oxide chain compound that exists within the $p(2\times1)$ structure. The binding energies obtained for various configurations on the 4×4-Pt(111) surface are reported in Table II. We first considered the addition of two oxygen atoms to the $p(2\times1)$ structure, which results in a coverage of 0.625 ML, and compared clustered versus nonclustered arrangements of the extra oxygen atoms (see Fig. 8). We find that the additional O atoms prefer to bind near

TABLE II. Binding energies of surface O and subsurface O configurations on 4×4-Pt(111). (a),(b) =tetra-I,-II site. (c),(nc)=clustered, nonclustered.

Sites	Θ_{total} (ML)					
on-surface/sub-surface	0.25	0.50	0.5625	0.6250	0.6875	0.75
Nonbuckled Pt surface O configurations						
(*n*)fcc/-	1.21	0.90	0.80	0.70	0.61	0.52
(*n*-1)fcc+1 hcp/-	1.09	0.82				
Buckled Pt surface O configurations						
(*n*-1)fcc+1 hcp/-			0.84			
				0.83 (c)		
(*n*-2)fcc+2 hcp/-				0.77 (nc)		
(*n*-3)fcc+3 hcp/-					0.80	
						0.82 (c)
(*n*-4)fcc+4 hcp/-						0.62 (nc)
Subsurface O configurations						
		0.67 (a)	0.68 (a)			
(*n*-1)fcc/tetra-I	0.73	0.78 (b)	0.77 (b)			
				0.73 (c)		
(*n*-2)fcc+1 hcp/tetra-I				0.70 (nc)		
				0.69 (c)		
(*n*-2)fcc/2 tetra-I				0.66 (nc)		
						0.52 (c)
(*n*-4)fcc+3 hcp/tetra-I						0.50 (nc)
						0.45 (c)
(*n*-4)fcc/4 tetra-I						0.51 (nc)
		0.67 (a)	0.70 (a)			
(*n*-1)fcc/tetra-II		0.63 (b)	0.63 (b)			
(*n*-4)fcc+3 hcp/tetra-II						0.44 (b)

hcp sites and aggregate between the close-packed oxygen rows formed by the $p(2\times1)$ structure [Fig. 8(a)]. The clustered surface configuration is favored over the all-fcc and nonclustered configurations by 0.13 and 0.06 eV/O atom, respectively. Similarly, clustering of the subsurface O atoms is slightly favored, but the surface configuration is found to be favored over subsurface by 0.1 eV/O atom. As seen in Fig. 8(a), the clustered surface configuration produces an oxide chain containing three outwardly displaced Pt atoms. Thus, extending the Pt oxide chain in this case involves buckling of only one additional Pt atom, and results in a structure with two Pt atoms each with threefold Pt-O coordination and one Pt atom with fourfold Pt-O coordination. In contrast, generating one of the nonclustered configurations involves buckling of two Pt atoms, which is more energetically demanding than displacing only one additional Pt atom out of the surface plane. Enhanced Pt-O bonding in the fourfold versus threefold-coordinated Pt species may also provide a driving force for oxygen aggregation and chain growth.

Figure 9(b) shows the most favored arrangement at 0.6875 ML associated with an extension of the oxide chain parallel to the $p(2\times1)$ rows. This configuration can be compared with the most favored arrangement reported at 2/3 ML for an all-fcc surface configuration,[13] which consists of maximally separated O atoms residing on fcc sites [Fig. 9(a)]. Despite the slightly greater surface coverage, the 0.6875 ML configuration has a 0.11 eV/O atom greater binding energy than the all-fcc 2/3 ML configuration, demonstrating that oxide chain growth is favored over the all-fcc configuration up to nearly 0.70 ML. In fact, the difference in energy between oxide chain structures and all-fcc surface configurations increases at higher coverages, which indicates that the oxide chain configurations become increasingly favored over maximally separated all-fcc configurations as the coverage increases above 0.50 ML. The final coverage that we examined on the 4×4-Pt(111) surface is 0.75 ML, and the clustered configuration is favored over the all-fcc configuration by a substantial 0.3 eV/O atom.

The increasing stability of the oxide chain with added O atoms can be more clearly observed by the energy gained from adding an O atom. We can define this added binding energy (E^n_{add}) by

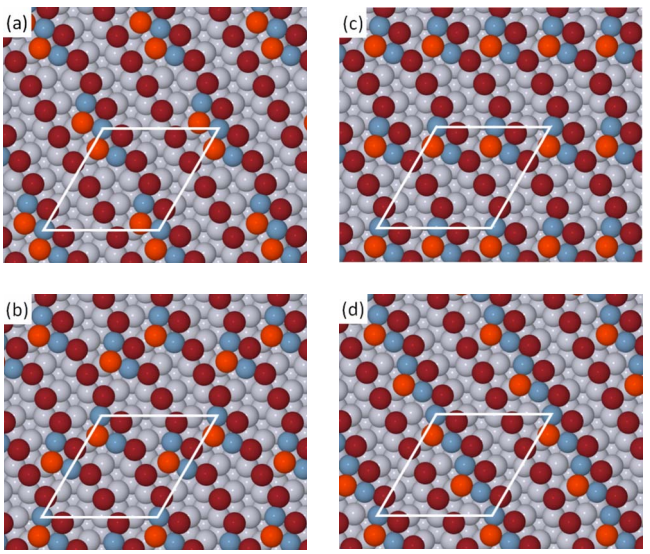

FIG. 8. (Color online) Top views of the most stable surface O atom configurations at 0.625 ML found on the 4×4 surface unit cell that illustrate the preference for O atoms added post-0.50 ML (orange) to cluster between $p(2\times1)$ rows (red). The gray and blue represent the down and up buckled Pt atoms, respectively. Clustered O (a) is favored by 0.06 eV/O atom to nonclustered O (c) and 0.08 eV/O atom to (b) and (d).

$$E^{n}_{\mathrm{add}} = E^{n-1}_{\mathrm{O/Pt}} + E_{\mathrm{O_2}}/2 - E^{n}_{\mathrm{O/Pt}}, \tag{2}$$

where n and $n-1$ refer to the number of O atoms in the O/Pt(111) structure. E^{n}_{add} is a measure of the stability gained by the system upon the addition of one O atom, where, by our definition, a positive value for E^{n}_{add} indicates increased stability. The added binding energy for the buckled structure at 0.5625 ML is 0.33 eV, which increases to 0.73 eV for the buckled structure at 0.625 ML. This increase suggests a large stability to growing the oxide chain from the initial nucleation. At 0.6875 ML, E^{n}_{add} drops to a value of 0.52 eV, which can be attributed to interactions with the periodic image in our relatively small unit cell. To more accurately probe the stability of the chain with increasing length will require larger unit cells and is the focus of current work. In contrast to the stability gained by the oxide chains with O atom addition, when we examine E^{n}_{add} values for all-fcc surface configurations, we find a destabilizing effect upon addition of O atoms beyond 0.5 ML. At 0.5625 ML, the added binding energy is −0.03 eV for the all-fcc surface configuration, and this value steadily decreases with subsequent O atom addition to −0.44 eV at 0.75 ML.

Figure 10 shows a comparison between the oxide chain configuration and the all-fcc configuration at 0.75 ML, and several differences are clear. First, the use of a 4×4-Pt(111) surface cell allows us to arrange the four additional oxygen atoms in a chain configuration between the oxygen rows of the $p(2\times1)$ structure at 0.75 ML. At the same coverage on the 2×2-Pt(111) system, we are restricted to adding one oxygen atom that results in a configuration where the oxygen atoms are separated to a maximum distance. The result of this more separated configuration is that the surface does not buckle [see Fig. 10(b)]. In contrast, the clustered configuration results in massive buckling (1.79 Å) of the Pt atoms located between the added row of oxygen atoms and the close-packed oxygen row of the $p(2\times1)$. This buckling and formation of an oxide chain allows the oxygen atoms to be screened from one another and reduces the O-O repulsion that would be normally found on oxygen surface configurations. The net effect of the buckling is an oxide chain configuration, which involves oxygen clustering instead of the separation of the oxygen atoms. Furthermore, the predicted chain structures closely resemble the chains that have been identified by STM at coverages greater than 0.40 ML. In particular, the STM images indicate oxide chain growth along $p(2\times1)$ rows and a buckling of 1.7 Å, which compares well with our value of 1.79 Å.

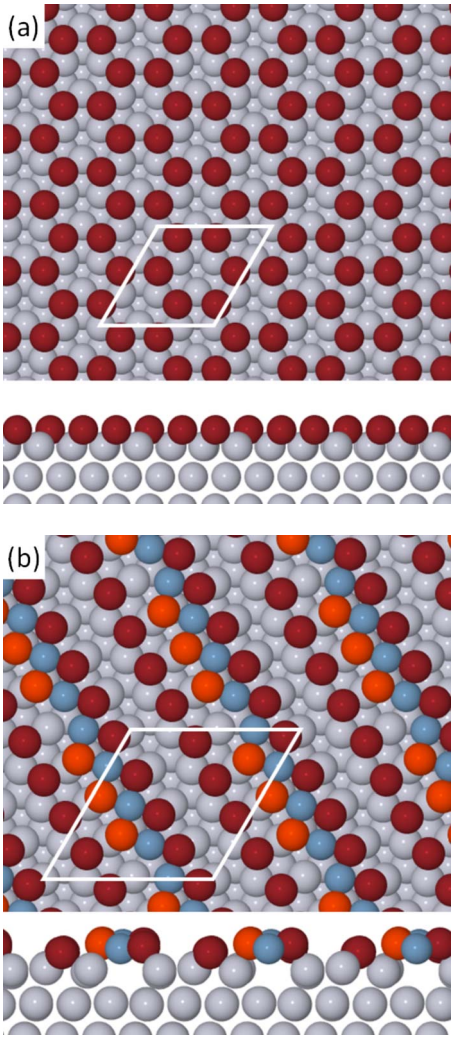

FIG. 9. (Color online) Top and side views of (a) the most stable surface all-fcc O atom configurations at 2/3 ML on the 3×3 surface unit cell and (b) the most stable O atom configuration at 0.6875 ML on the 4×4 surface unit cell. In (a), O atoms are arranged in a $p(\sqrt{3}\times\sqrt{3})$-2O configuration; in (b), O atoms forming $p(2\times1)$ rows are red, and those added post-0.50 ML are orange. The gray and blue represent the down and up buckled Pt atoms, respectively. The striped structure (b) is favored by 0.08 eV/O atom to the hexagonal structure (a). The Pt buckling in (b) is 1.75 Å.

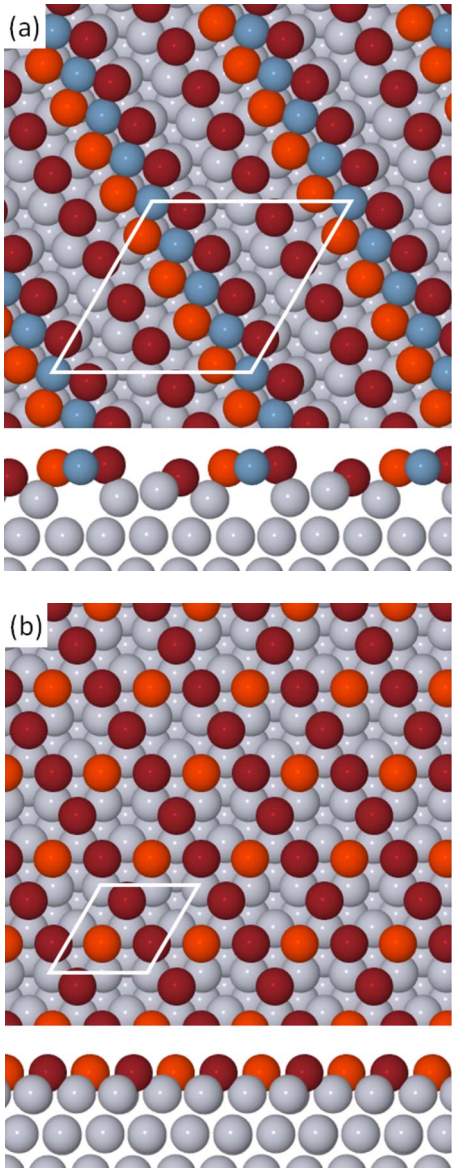

FIG. 10. (Color online) Top and side views of the most stable surface O atom configurations at 0.75 ML found on (a) the 4×4 surface unit cell and (b) the 2×2 surface unit cell. O atoms forming $p(2\times1)$ rows are red, and those added post-0.50 ML are orange. The gray and blue represent the down and up buckled Pt atoms, respectively. The striped structure (a) is favored by 3.59 eV (0.30 eV/O atom) to the symmetric structure (b). The Pt buckling in (a) is 1.79 Å.

As mentioned above, the chain structures do not represent a chemisorbed state but are better described as a Pt oxide chain compound that serves as a precursor to the formation of a full two-dimensional (2D) or three-dimensional (3D) oxide on the Pt(111) surface, as demonstrated in prior experimental studies.[5,19] The nearly 2 Å buckling of the Pt atoms out of the surface suggests that chain formation may be viewed as a chemical reaction involving the cleavage of Pt-Pt bonds between the first and second layer Pt atoms and the concurrent formation of Pt-O bonds. Moreover, the Pt atoms within the chains experience fourfold coordination with oxygen atoms, forming square planar units that closely resemble the building blocks of bulk PtO, Pt_3O_4 and α-PtO_2. Thus, following Devarajan *et al.*,[19] we refer to the 1D metal oxide compound as Pt oxide chains. However, it is important to stress that the structures we have identified in our 4×4-Pt(111) calculations are not a full representation of the experimental STM images obtained after the chains have grown appreciably. In the DFT calculations, the periodic boundary conditions and the use of a 4×4-Pt(111) system results in an infinitely long Pt oxide chain at 0.75 ML running parallel to the $p(2\times1)$ rows. In contrast, the STM results show that the chains aggregate and eventually arrange into an interconnected network of Y-shaped structures near 0.75 ML, where each leg of the Y structure consists of two to three side-by-side Pt oxide chains with lengths between 19 and 24 Å. Minimizing interfacial stresses must be responsible for the narrow distribution of chain lengths and the development of the chain superstructure. In particular, lattice mismatch between the Pt oxide chains and the Pt(111) substrate causes stress to build up along the Pt oxide chains. Termination of the chain length and chain branching likely relieves this stress, resulting in the narrow distribution of chain lengths and branched superstructure observed experimentally. Unfortunately, however, the interfacial stresses cannot be relieved adequately in our DFT supercells due to the characteristic large length scales of the chain superstructures. Future DFT calculations with larger supercells will be needed to quantify these strain effects. Interestingly, the 0.75 ML Pt oxide chain structure has a slightly larger binding energy than at 0.6875 ML (0.82 versus 0.80 eV/O atom), which suggests that the oxide chain should prefer to grow until the optimal length is reached to minimize strain effects.

Based on the finding of oxide chain growth on Pt(111), we revisited the 2×2-Pt(111) system at 1 ML. Originally, as detailed in Sec. III A, we examined mixed surface configurations by considering $(n-1)$ fcc hollow sites and 1 hcp hollow site. Following this procedure, we found that the all-fcc 1 ML configuration is favored over three O atoms on fcc hollows and one O atom on an hcp hollow site. If instead we allow two O atoms to reside on fcc hollows [the $p(2\times1)$ structure] and add two O atoms to the hcp sites in between the $p(2\times1)$ rows, the resulting mixed surface configuration is more stable by 0.36 eV/O atom. The resulting relaxed structure is shown in Fig. 11(a), and we can observe the formation of a surface-oxide phase that is quite distinct from chemisorbed oxygen atoms or subsurface oxygen (see Figs. 2 and 3). The configuration shows substantial buckling of both O and Pt surface atoms and can be considered a 2D oxide phase. In fact, a comparison of this structure with the α-PtO_2(0001) surface [Fig. 11(b)] shows that the two surfaces have very similar geometric structures. Recall that the α-PtO_2(0001) oxide film is predicted by DFT to be the stable oxide structure on Pt(111).[21,22]

Figure 12 summarizes the binding energies of the most favored surface and subsurface configurations we have identified using DFT on both the 2×2- and 4×4-Pt(111) surface cells. Interestingly, the binding energy for the Pt oxide structures drops quite sharply from 0.75 ML and 1 ML coverages. The main difference between the structures of the 0.75 ML 4×4-Pt(111) and 1 ML 2×2-Pt(111) is the reduction in the distance between parallel Pt oxide chains [compare Figs.

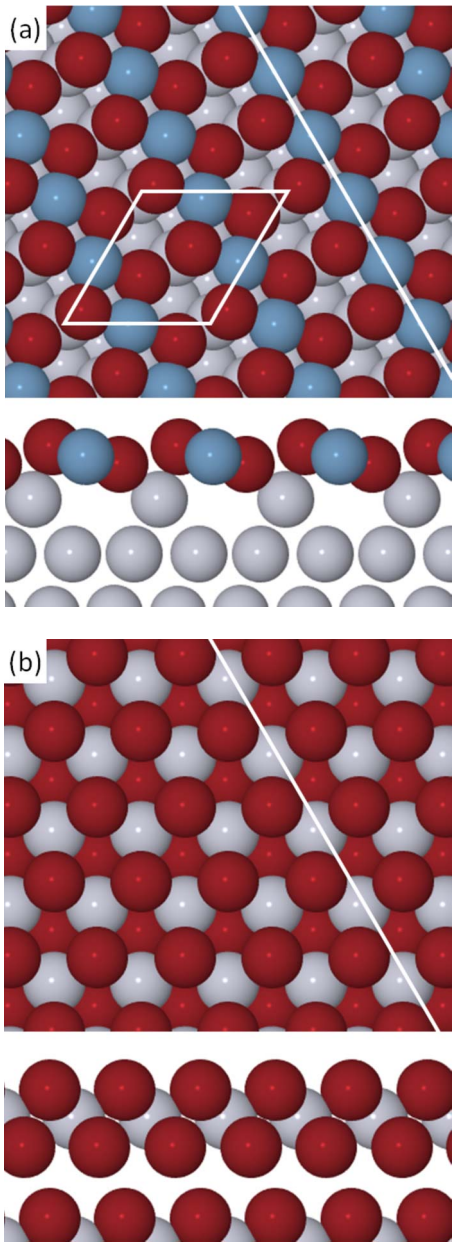

FIG. 11. (Color online) Top and side views of (a) the most stable surface O atom configuration at 1 ML found on the 2×2 surface unit cell, with $\frac{1}{2}$ occupying fcc sites and $\frac{1}{2}$ occupying hcp sites in a PtO_2-like structure, and (b) α-$PtO_2(0001)$. The O atoms are represented by red, and the gray and blue represent the down and up buckled Pt atoms, respectively. The Pt buckling in (a) is 1.64 Å. The line illustrates a 1D PtO_2 chain.

10(a) and 11(a)], which indicates a repulsive interaction between Pt oxide chains for the configuration shown in Fig. 11(a). However, because chain pairing is observed with STM at high coverages,[19] the predicted destabilization suggests that an optimum arrangement of side-by-side chains is not obtained using the 2×2 unit cell. For example, the oxygen atoms in adjacent chains lie in close proximity to one another in the 1 ML structure obtained with the 2×2 unit cell [Fig. 11(a)]. Indeed, the structure of the α-$PtO_2(0001)$ surface [Fig. 11(b)] suggests that the chain-chain interaction could become favorable if one of the chains is displaced along the chain direction. Larger supercells are likely to be needed to obtain an optimum configuration of chain pairs since the chains would be able to relax both parallel and perpendicular to the chain direction.

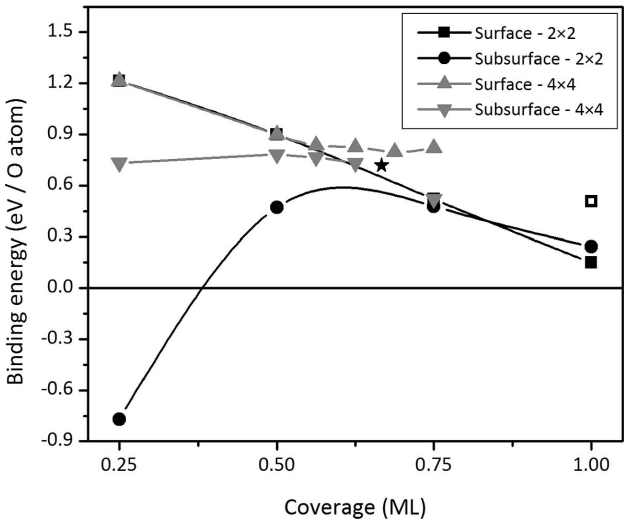

FIG. 12. Binding energy as a function of O coverage on 2×2- and 4×4-Pt(111) for the most stable surface (■,▲) and subsurface (●,▼) configurations. The binding energies for 1 ML $O/2\times2$-Pt(111) with $\frac{1}{2}$ occupying fcc sites and $\frac{1}{2}$ occupying hcp sites in a PtO_2-like structure (□) and 2/3 ML $O/3\times3$-Pt(111) [$p(\sqrt{3}\times\sqrt{3})$-2O] (★) are also included.

The primary changes in the structure of the oxide chain with increasing coverage is captured in Table III, where both the Pt-Pt bond distances within the oxide chains and the Pt buckling are reported. A clear trend of the Pt-Pt bond lengths approaching similar bond lengths to the bulk oxide surface can be observed as the surface oxygen coverage is increased beyond 0.5 ML to 0.75 ML. This observation reinforces the expectation that strain relief plays a large role in dictating the optimal chain lengths and oxide chain/Pt(111) substrate commensurability. At 0.75 and 1 ML the oxide structure is restricted to the in-plane lattice constant of Pt(111) and therefore cannot expand laterally to the more optimal lattice

TABLE III. Selected structural data for bare Pt(111), buckled Pt atoms along oxide chains, and α-$PtO_2(0001)$. Pt-Pt bond lengths are between buckled Pt atoms in the first Pt layer, and Pt buckling is the displacement in the surface-normal direction of Pt atoms in the first Pt layer.

Structure	Pt-Pt bond length (Å)	Pt buckling (Å)
Bare Pt(111)	2.812	0.00
0.5625 ML O/Pt(111)	2.940	1.44
0.625 ML O/Pt(111)	3.000	1.77
0.6875 ML O/Pt(111)	2.916	1.75
0.75 ML O/Pt(111)	2.812	1.79
1 ML O/Pt(111)	2.812	1.64
α-$PtO_2(0001)$	3.082	

TABLE IV. Atomic charges of surface O on Pt(111) as a function of O coverage and α-PtO_2 (given in units of electrons). For O coverages above 0.50 ML where oxide chain structures are observed, values for $q_{Pt,down}$ outside the parentheses indicate the atomic charges of Pt atoms surrounding the upward-buckled Pt atoms that are coordinated to two O atoms, while values inside parentheses indicate the atomic charges of bulk-like Pt atoms in the first layer that are coordinated to only one O atom. Buckled Pt configurations are denoted with *.

Coverage (ML)		q_O	q_{Pt} up	q_{Pt} down
0.25		−0.75	0.25	−0.05
0.50		−0.76	0.54	0.24
0.5625*		−0.77	0.90	0.53 (0.24)
0.625	clustered*	−0.78	0.87/1.17	0.54 (0.24)
	not clustered*	−0.78	0.91	0.53 (0.24)
0.6875*		−0.80	1.00	0.46 (0.26)
0.75	all fcc	−0.74	0.52	0.80
	$\frac{1}{2}$fcc+$\frac{1}{4}$hcp*	−0.82	1.14	0.63 (0.36)
1	all fcc	−0.71	0.78	
	$\frac{1}{2}$fcc+$\frac{1}{2}$hcp*	−0.84	1.26	0.44
Bulk α-PtO_2		−0.82	1.64	
α-PtO_2(0001)		−0.82	1.64	

constant for the oxide chains. Even with this artificial constraint, the chain structures are substantially more stable than chemisorbed oxygen structures at coverages above 0.50 ML. The buckling of the Pt does not dramatically change with coverage, except at 1 ML, where the buckling becomes slightly less pronounced, reflecting oxide-oxide interactions perpendicular to the Pt oxide chains. The buckling observed in our DFT results agree well with the value of 1.7 Å reported in the STM study.[19]

We conclude the paper by examining the atomic charges on the O and Pt atoms in the various configurations. We mentioned above that the chain structures better resemble a Pt oxide compound rather than a chemisorbed state of oxygen on Pt(111). This classification is evident from the geometric structure but should also be reflected in the electronic structure. Table IV reports the atomic charge values, obtained from a Bader analysis of the charge density,[39–41] for surface O and Pt atoms in various surface configurations as a function of coverage. Table IV also includes the atomic charges for bulk α-PtO_2 and the α-PtO_2(0001) surface. Since the PtO_2 trilayers in bulk α-PtO_2 are separated by about 4.5 Å and interact only through weak van der Waals forces,[42] it is not surprising that the atomic charges for the α-PtO_2(0001) surface are very nearly equal to those of bulk α-PtO_2. An examination of the charge on the O atom shows that the O atoms in the Pt oxide chain structures have slightly more negative charge than the all-fcc nonclustered configurations. The O atom charge in the clustered configurations increases with increasing coverage as these structures become more Pt oxidelike, and at coverages of 0.75 and 1 ML the O atom charge is the same as in the α-PtO_2 oxide.

A much larger charge difference is found on the Pt atoms. For the all-fcc configurations, the small Pt buckling results in charge differences between the up and down surface Pt atoms of approximately 0.30 electrons. This charge difference between up and down Pt atoms is more pronounced for configurations with more fully developed Pt oxide chains (0.75 and 1 ML), where we find a 0.5 and 0.8 electron difference, respectively. Furthermore, the up Pt atoms of the chains are more positively charged than those found in the chemisorbed oxygen phase. The more positively charged Pt atom screens the negatively charged oxygen atom and results in oxidelike bonding in these structures. Similar arguments have been recently invoked to describe oxide chains on Pt(110),[43] oxide formation along the step edges on Pt(332),[44] and oxygen and sulfur-induced restructuring of Au(111) surfaces.[45–47] Therefore, the evidence suggests that oxide compound formation can be induced on a range of metal surfaces through charge transfer and overcomes the penalty in buckling the metal or breaking metal-metal bonds. Based on the work on Pt(332), Wang and co-workers[44] suggested that the Pt oxide chains forming on step edges might be a precursor to bulk oxide formation, but our results demonstrate that oxide chains can form on Pt(111) terraces as well, which implies that bulk oxide formation does not necessarily initiate only at step edges of Pt surfaces. The reactivity of the 1D Pt oxide chains could be quite distinct from chemisorbed O atoms on Pt(111) and could impact the present understanding of CO and NO oxidation on Pt surfaces.

IV. SUMMARY AND CONCLUSIONS

Using DFT we have identified Pt oxide chain structures that develop on Pt(111) at oxygen coverages beyond 0.5 ML that are more stable than previously reported configurations of chemisorbed oxygen atoms.[12,13] Formation of the Pt oxide chains involves oxygen atoms binding near hcp sites and forming close-packed rows that run parallel to the $p(2\times1)$ oxygen rows. The oxygen atoms in the added rows induce strong buckling of the Pt surface atoms which allows for screening of the repulsive O-O interactions and stabilizes the structure. An analysis of the atomic charges shows that the Pt atoms in the chain structures are quite distinct from Pt atoms bonded to chemisorbed oxygen atoms and are more properly termed 1D Pt oxide chains. The structures we have identified reproduce many of the features of recent STM images of O/Pt(111).[19]

Based on the identified structures and the STM work, we can roughly describe the evolution of oxygen phases on Pt(111) up to an oxygen coverage of 0.75 ML. At low coverages ($\leq$ 0.25 ML), the oxygen atoms arrange in a $p(2\times2)$ structure. With additional O atoms, a $p(2\times1)$ structure starts to form and co-exists with the $p(2\times2)$ phase. As the coverage starts to approach 0.5 ML, it becomes increasingly dominated by the $p(2\times1)$ phase. On the $p(2\times1)$ domains, we begin to observe oxygen atoms aggregating and growing Pt oxide chains that run parallel to the $p(2\times1)$ oxygen rows. Prior STM images show that the chains form Y-shaped structures that restrict the lengths of the chains (see Ref. 19 for more details). Our DFT results for

1 ML coverage and earlier studies of oxide films on Pt(111) (Refs. 21 and 22) suggest that the chains eventually merge and transition into a 2D $PtO_2(0001)$ film that is rotated by 30° with respect to Pt(111). We note that similar oxide compound formation has been reported on Au(111),[45,46] Pt(110),[43] and along steps on Pt(332).[44] These results suggest that the initiation of oxide formation on metal surfaces is the development of low-dimensional metal oxide compounds that induce large metal atom buckling and are stabilized by large charge transfer. Such oxide structures form at even moderate oxygen coverages and could play an important role in the catalytic behavior of these metal surfaces.

While we have gained a better understanding of oxygen phase evolution on Pt(111), there are still several open questions that need to be further addressed. It is important to stress that the structures that we have identified on the 4×4-Pt(111) surface do not fully represent the true experimental picture. Experimental STM images show that at coverages approaching 0.75 ML, the chains form an interconnected network of Y-shaped structures with each chain 19 to 24 Å long. Fully reproducing the long-range chain network observed in experiment is beyond the scope of DFT due to size limitations. We are currently extending our examination of the growth of the oxide chains through the use of larger surface unit cells. While such surface cells cannot incorporate Y structures, they should allow us to probe chain-chain interactions and preferred chain growth directions and possibly chain lengths. A combination of such studies with comparisons between DFT-derived and experimental STM should assist in better understanding the formation and growth of the oxide chains.

More studies, both experimental and modeling, are needed to fully explore the transition of Pt oxide chains to a full 2D PtO_2 film on Pt(111). The findings from this study already have important implications for proposed models of NO oxidation on Pt(111),[14,48,49] where NO oxidation on chemisorbed O surface phases was examined. Our work suggests that NO oxidation on the Pt oxide chains should also be examined since these structures form at relatively modest oxygen coverages. Potentially, the presence of the Pt oxide chains plays an important role in the observed NO reactivity at coverages near 0.5 ML.[14,48,49] The results on Pt(111) also suggest that the initial stages of the oxidation of Pd(111) should be revisited. DFT studies found that subsurface O becomes favorable on Pd(111) above 0.5 ML,[20] but 2D oxide structures form before those surface coverages are reached.[10,50,51] It will be interesting to determine if oxygen atom clustering plays a similar role in bulk oxide formation on Pd(111) as on Pt(111). Finally, the present study points to the difficulty of relying solely on DFT to predict surface structures in strongly reactive systems, such as oxygen on TM surfaces. Studies of the oxidation of TM surfaces show that quite complex and difficult to predict configurations often form at even moderate oxygen coverages.

ACKNOWLEDGMENTS

We acknowledge the University of Florida High-Performance Computing Center (http://hpc.ufl.edu) for providing computational resources for performing some of the calculations reported in this paper. A.A. acknowledges support from ACS-PRF under Grant No. 47596-G5, and J.F.W. acknowledges support from NSF-CBET through Grant No. NSF-CAREER CTS-0348287.

*Corresponding author. aasthagiri@che.ufl.edu

[1] J. F. Weaver, H. H. Kan, and R. B. Shumbera, J. Phys.: Condens. Matter **20**, 184015 (2008).
[2] D. H. Parker, M. E. Bartram, and B. E. Koel, Surf. Sci. **217**, 489 (1989).
[3] N. Saliba, Y. L. Tsai, C. Panja, and B. E. Koel, Surf. Sci. **419**, 79 (1999).
[4] R. B. Shumbera, H. H. Kan, and J. F. Weaver, Surf. Sci. **601**, 4809 (2007).
[5] J. F. Weaver, J. J. Chen, and A. L. Gerrard, Surf. Sci. **592**, 83 (2005).
[6] C. R. Parkinson, A. Walker, and C. F. McConville, Surf. Sci. **545**, 19 (2003).
[7] M. S. Chen, Y. Cal, Z. Yan, K. K. Gath, S. Axnanda, and D. W. Goodman, Surf. Sci. **601**, 5326 (2007).
[8] E. Lundgren, J. Gustafson, A. Resta, J. Weissenrieder, A. Mikkelsen, J. N. Andersen, L. Kohler, G. Kresse, J. Klikovits, A. Biederman, M. Schmid, and P. Varga, J. Electron Spectrosc. Relat. Phenom. **144-147**, 367 (2005).
[9] J. Gustafson, A. Mikkelsen, M. Borg, E. Lundgren, L. Kohler, G. Kresse, M. Schmid, P. Varga, J. Yuhara, X. Torrelles, C. Quiros, and J. N. Andersen, Phys. Rev. Lett. **92**, 126102 (2004).
[10] E. Lundgren, G. Kresse, C. Klein, M. Borg, J. N. Andersen, M. De Santis, Y. Gauthier, C. Konvicka, M. Schmid, and P. Varga, Phys. Rev. Lett. **88**, 246103 (2002).
[11] J. Klikovits, E. Napetschnig, M. Schmid, N. Seriani, O. Dubay, G. Kresse, and P. Varga, Phys. Rev. B **76**, 045405 (2007).
[12] P. Legare, Surf. Sci. **580**, 137 (2005).
[13] R. B. Getman, Y. Xu, and W. F. Schneider, J. Phys. Chem. C **112**, 9559 (2008).
[14] S. Ovesson, B. I. Lundqvist, W. F. Schneider, and A. Bogicevic, Phys. Rev. B **71**, 115406 (2005).
[15] A. Eichler, F. Mittendorfer, and J. Hafner, Phys. Rev. B **62**, 4744 (2000).
[16] H. R. Tang, A. Van der Ven, and B. L. Trout, Phys. Rev. B **70**, 045420 (2004).
[17] H. R. Tang, A. Van der Ven, and B. L. Trout, Mol. Phys. **102**, 273 (2004).
[18] D. I. Jerdev, J. Kim, M. Batzill, and B. E. Koel, Surf. Sci. **498**, L91 (2002).
[19] S. P. Devarajan, J. A. Hinojosa, Jr., and J. F. Weaver, Surf. Sci. **602**, 3116 (2008).
[20] M. Todorova, K. Reuter, and M. Scheffler, Phys. Rev. B **71**, 195403 (2005).
[21] N. Seriani, W. Pompe, and L. C. Ciacchi, J. Phys. Chem. B **110**, 14860 (2006).

[22] N. Seriani and F. Mittendorfer, J. Phys.: Condens. Matter **20**, 184023 (2008).
[23] G. Kresse and J. Furthmuller, Comput. Mater. Sci. **6**, 15 (1996).
[24] G. Kresse and J. Furthmuller, Phys. Rev. B **54**, 11169 (1996).
[25] G. Kresse and J. Hafner, Phys. Rev. B **49**, 14251 (1994).
[26] G. Kresse and J. Hafner, Phys. Rev. B **47**, 558 (1993).
[27] G. Kresse and D. Joubert, Phys. Rev. B **59**, 1758 (1999).
[28] P. E. Blochl, Phys. Rev. B **50**, 17953 (1994).
[29] J. P. Perdew, K. Burke, and M. Ernzerhof, Phys. Rev. Lett. **77**, 3865 (1996).
[30] M. Methfessel and A. T. Paxton, Phys. Rev. B **40**, 3616 (1989).
[31] D. Sheppard, R. Terrell, and G. Henkelman, J. Chem. Phys. **128**, 134106 (2008).
[32] H. J. Monkhorst and J. D. Pack, Phys. Rev. B **13**, 5188 (1976).
[33] A. D. Polli, T. Wagner, T. Gemming, and M. Rühle, Surf. Sci. **448**, 279 (2000).
[34] R. A. Olsen, G. J. Kroes, G. Henkelman, A. Arnaldsson, and H. Jonsson, J. Chem. Phys. **121**, 9776 (2004).
[35] G. Henkelman, B. P. Uberuaga, and H. Jonsson, J. Chem. Phys. **113**, 9901 (2000).
[36] G. Henkelman and H. Jonsson, J. Chem. Phys. **113**, 9978 (2000).
[37] Z. H. Gu and P. B. Balbuena, J. Phys. Chem. C **111**, 9877 (2007).
[38] D. C. Ford, Y. Xu, and M. Mavrikakis, Surf. Sci. **587**, 159 (2005).
[39] G. Henkelman, A. Arnaldsson, and H. Jonsson, Comput. Mater. Sci. **36**, 354 (2006).
[40] E. Sanville, S. D. Kenny, R. Smith, and G. Henkelman, J. Comput. Chem. **28**, 899 (2007).
[41] W. Tang, E. Sanville, and G. Henkelman, J. Phys.: Condens. Matter **21**, 084204 (2009).
[42] T. M. Pedersen, W. X. Li, and B. Hammer, Phys. Chem. Chem. Phys. **8**, 1566 (2006).
[43] S. Helveg, H. T. Lorensen, S. Horch, E. Laegsgaard, I. Stensgaard, K. W. Jacobsen, J. K. Norskow, and F. Besenbacher, Surf. Sci. **430**, L533 (1999).
[44] J. G. Wang, W. X. Li, M. Borg, J. Gustafson, A. Mikkelsen, T. M. Pedersen, E. Lundgren, J. Weissenrieder, J. Klikovits, M. Schmid, B. Hammer, and J. N. Andersen, Phys. Rev. Lett. **95**, 256102 (2005).
[45] B. K. Min, A. R. Alemozafar, M. M. Biener, J. Biener, and C. M. Friend, Top. Catal. **36**, 77 (2005).
[46] J. Biener, M. M. Biener, T. Nowitzki, A. V. Hamza, C. M. Friend, V. Zielasek, and M. Baumer, ChemPhysChem **7**, 1906 (2006).
[47] M. M. Biener, J. Biener, and C. M. Friend, Langmuir **21**, 1668 (2005).
[48] R. B. Getman and W. F. Schneider, J. Phys. Chem. C **111**, 389 (2007).
[49] A. D. Smeltz, R. B. Getman, W. F. Schneider, and F. H. Ribeiro, Catal. Today **136**, 84 (2008).
[50] G. Zheng and E. I. Altman, Surf. Sci. **462**, 151 (2000).
[51] H. Gabasch, W. Unterberger, K. Hayek, B. Klotzer, G. Kresse, C. Klein, M. Schmid, and P. Varga, Surf. Sci. **600**, 205 (2006).